Evaluation of the Purity of Magnesium Hydroxide Recovered from Saltwork Bitterns

Giuseppe Battaglia [1], Maria Alda Domina [1], Rita Lo Brutto [2], Julio Lopez Rodriguez [3],
Marc Fernandez de Labastida [3], Jose Luis Cortina [3], Alberto Pettignano [2], Andrea Cipollina [1,*],
Alessandro Tamburini [1] and Giorgio Micale [1]

1   Dipartimento di Ingegneria, Università degli Studi di Palermo (UNIPA), Viale delle Scienze,
    90128 Palermo, Italy
2   Dipartimento di Fisica e Chimica—Emilio Segrè, Università degli Studi di Palermo (UNIPA),
    Viale delle Scienze, 90128 Palermo, Italy
3   UPC-BarcelonaTECH, 08930 Barcelona, Spain
*   Correspondence: andrea.cipollina@unipa.it

Abstract: Magnesium has been listed among the 30 critical raw materials by the European Union. In recent years, many green and sustainable alternative Mg^{2+} sources have been sought to satisfy the EU's demand and to avoid mineral ore consumption. In this context, saltwork bitterns, the by-products of solar sea salt production, have attracted much attention thanks to their high Mg^{2+} concentrations (up to 80 g/L) and low Ca^{2+} and bicarbonate contents (<0.5 g/L). Although investigations on Mg^{2+} extraction from bitterns in the form of $Mg(OH)_2(s)$ have already been performed, product purity has never been properly addressed. $Mg(OH)_2(s)$ is a chemical compound of great interest and extensive utility in numerous industrial applications only if the powder's purity is >95% (*w/w*). This work presents a comprehensive experimental effort of reactive precipitation tests with NaOH solutions at stoichiometric and over-stoichiometric concentrations to: (i) assess the technical feasibility of Mg^{2+} recovery from real bitterns collected in saltworks of the Trapani district (Italy) and, (ii) for the first time, conduct an extensive purity investigation of the precipitated magnesium hydroxide powders as brucite. This experimental investigation demonstrates the possibility of extracting highly valuable compounds from saltwork bittern waste, embracing the water valorization and resource recovery approach.

Keywords: $Mg(OH)_2(s)$; brucite; precipitation; mineral recovery; circular economy; seawater valorization

1. Introduction

Magnesium hydroxide (MH, $Mg(OH)_2$) is a chemical compound widely employed in numerous industrial fields [1]. In the last decade, MH has been established as a promising flame-retardant agent thanks to its degradation properties, and smoke- and toxic-free characteristics [2]. Furthermore, it has been extensively used as an antibacterial agent, a neutralization reagent of acidic liquid waste, as an environmentally friendly material for reducing the water pollution of heavy metals [3], as a paper preservative and as a precursor for magnesium oxide preparation [4–6]. Nowadays, commercial MH products are mainly obtained from minerals (e.g., from serpentinite rock via the Magnifin process [7]), bischofite brines [7] and seawater using dolomitic lime [8,9]. These processes are high-energy-demanding and generate mineral depletion with a significant impact on the environment. The worldwide market of MH is foreseen to reach 932,000 tonnes by 2022 with a compound annual growth rate (CAGR) of 3.4% over 2016–2022, clearly marking a continuous, growing and attractive market [7]. However, the increasing mineral depletion and environmental concerns regarding the $CO_2(g)$ footprint of obtaining MH from conventional sources have pushed researchers and industrials to seek alternative Mg^{2+} sources.

Turek and Gnot [10], already in 1995, proposed a two-step process for the purification of hard coal mine brines produced by coal mines in Poland. The idea was to purify the coal brines while extracting, at the same time, high-added-value minerals. The brines contained 2.84 g/L of Mg^{2+}, which was recovered via precipitation in the form of MH. In the last decade, increasing interest has been placed on seawater desalination [11–13] and the high magnesium content in lake brines, as in the case of the Uyuni salar (Bolivia), which is one of the largest sources of lithium and also contains 15–18 g/L of Mg^{2+} [14,15].

Magnesium is the third most abundant element in seawater after sodium and chloride. It has a typical concentration of about 1.3 g/L, and its concentration almost doubles in seawater reverse osmosis desalination brines. Zhang et al. [16], in their recent review, highlighted the exponential increment of publications dealing with the topic of resource recovery focused on the exploitation of seawater desalination brines. The reasons behind that are the high Mg^{2+} concentration in brines and the ever-growing installed capacity of desalination plants worldwide for the production of potable water, with the associated brines being rejected.

Mg^{2+} is typically recovered from seawater brine as magnesium hydroxide via precipitation employing an alkaline reagent [16]. Besides MH, several Mg^{2+} compounds have been produced from concentrated brines and wastewaters such as struvite $(NH_4)MgPO_4 \cdot 6(H_2O)(s))$ [17,18], magnesium sulphate $(MgSO_4 7H_2O(s))$ [19], and magnesium oxide $(MgO(s))$ [20,21]. Furthermore, many alternative processes have been proposed to extract Mg^{2+} using electro-membrane applications [22,23] or organic systems containing ionic liquids [24].

Although, seawater and seawater brine represent a sustainable Mg^{2+} resource, the recovery of Mg^{2+} from such sources is hindered by the presence of many dissolved ions. The presence of HCO_3^- and Ca^{2+} ions can cause the precipitation of calcium carbonate $(CaCO_3(s))$ as calcite or aragonite at solution pH values above nine. In addition, if hydroxyl ions and sulphate ions are dissolved in the solution, calcium can precipitate as calcium hydroxide $(Ca(OH)_2(s))$ or calcium sulphate $(CaSO_4 \cdot 2H_2O(s))$, affecting the purity of the recovered Mg^{2+} compounds [21,25].

Gong et al. [26] investigated the feasibility of mineral recovery from seawater brines. The authors marked the high economic, social and environmental benefits associated with the brine's exploitation. Brines from the Perth seawater desalination plant (Perth, Australia) were treated using lime as a precipitant to recover Mg^{2+} as MH. Low $Mg(OH)_2(s)$ purity of ~70% was reported due to the presence of bicarbonates and calcium ions, while it was possible to reach values up to 91% only after a wet screening of the lime. Recently, Vassallo et al. [27] have proposed a novel crystallizer, using NaOH, for the selective recovery of Mg^{2+}, as MH, and Ca^{2+}, as calcium hydroxide, from the retentate of a nanofiltration unit treating spent brine from an industrial water production plant of Evides Industriewater B.V. (Rotterdam, The Netherlands). The spent brine had a concentration of 3 g/L of Mg^{2+} and 24 g/L of Ca^{2+}. The precipitation pH was carefully controlled during the process, leading to 100% Mg^{2+} and 97% Ca^{2+} recoveries with cationic purities above 95%. Morgante et al. [28] characterized the sedimentation and filtration properties of $Mg(OH)_2$ suspensions produced by adopting the same novel crystallizer. The influence of brine concentrations, solution flow rates and seeded precipitation (by-products recycled) were addressed. A marked beneficial influence was observed by adopting seeded precipitation that considerably reduced sedimentation times (up to four times) and enhanced filtration characteristics. In the study, only synthetic solutions were employed, and no purity analyses were conducted. The same research group also proposed an innovative technology to recover Mg^{2+} as MH from seawater and industrial waste brines. An innovative ionic exchange membrane crystallizer (Cr-IEM) was experimentally and numerically studied to recover Mg^{2+} in a controlled manner exploiting low-cost alkaline solutions, such as $Ca(OH)_2$ slurries [29,30]. The crystallizer employed an anionic membrane that allows the passage of only hydroxyl ions, preventing the flux of undesired cations such as, for example, Ca^{2+}. To reduce the impact of dissolved ions in brines, Yousefi et al. [31] studied the production of $Mg(OH)_2$

nanoflakes, using poly(ethylene glycol) (PEG 4000) as a surfactant, from the impure brine of Iranian evaporation ponds that contained ~50 g/L of Mg^{2+} and ~182 g/L of Ca^{2+} using NaOH. To produce a high-purity magnesium hydroxide (purity values ~86%), the authors carefully controlled the precipitation pH, which was kept between 9 and 9.5. This accurate pH control reduced the $Ca(OH)_2$ precipitation, with no impurity traces detected through X-ray diffraction (XRD).

The use of NaOH solutions as alkaline reactants for the recovery of $Mg(OH)_2$ from brines or seawater allows for the production of highly pure $Mg(OH)_2$ compounds. On the other hand, NaOH is an expensive reactant. As an alternative, the use of low-cost lime ($Ca(OH)_2$) suspensions is also possible and may lead, in principle, to high $Mg(OH)_2$ purity if suitable brine or seawater pre-treatments are adopted in order to reduce carbonates, calcium, and sulphate ions. In the literature, the following strategies have been reported: (i) the use of highly pure lime suspensions [32]; (ii) decarbonation of brines to avoid calcium carbonate precipitation by adding sulfuric acid (H_2SO_4) to lower the solution pH to four, combined with a carbon dioxide removal step using a desorption tower and a brine aerating process [32]; (iii) a controlled reaction with $Ca(OH)_2$ to precipitate soluble bicarbonate as insoluble calcium carbonate without $Mg(OH)_2$ precipitation [32]; and (iv) adoption of sodium carbonate (Na_2CO_3) and barium chloride ($BaCl_2$) solutions to precipitate calcium as calcium carbonate ($CaCO_3$) and sulphates as barium sulphate ($BaSO_4$) [33].

Among the unconventional sources of Mg^{2+}, bitterns represent a promising one. Bitterns are highly concentrated solutions and are typically by-products of the natural evaporation process of seawater from solar salt manufacturers. Lee et al. [34] evaluated the feasibility of exploiting bitterns for the production of struvite. They employed a food-grade bittern containing 32 g/L of Mg^{2+} and 8 g/L of Ca^{2+}. The bittern showed a similar performance as a Mg^{2+} source with respect to seawater for phosphate removal; however, it performed worse for ammonia removal. Alamdari et al. [35] performed fundamental research on MH precipitation kinetics from sea bittern. The authors studied the MH precipitation in seeded reactors using real and artificial solutions of 30 g/L of Mg^{2+}. A higher nucleation rate and a slower growth rate were inferred for MH precipitation from sea bitterns with respect to that from pure artificial solutions. Cipollina et al. [36] studied the potential Mg^{2+} recovery from bitterns collected from the final basins of the saltworks operating in the district of Trapani (Sicily, Italy). Experiments were performed both in semi-batch and continuous crystallizers treating a ~23 g/L bittern. A high $Mg(OH)_2$ purity and a total Mg^{2+} recovery (e.g., >99%) were reported. However, no details were provided regarding solid mass purity, which is a fundamental market requirement to be fulfilled.

The present work aims at filling this gap, thoroughly investigating Mg^{2+} recovery and, for the first time, precipitated $Mg(OH)_2(s)$ mass purity from real saltwork bitterns to pursue a strategy for valorizing waste bitterns as sustainable Mg^{2+} sources. Such bitterns are characterized by high Mg^{2+} content (>20 g/L) and very low Ca^{2+} and bicarbonate concentrations (<0.3 g/L) thanks to the fractionated precipitation process that occurs along the initial evaporative ponds [37]. Such low Ca^{2+} concentration makes them the perfect candidates for the recovery of high purity Mg^{2+} compounds. This research is carried out within the framework of the EU-funded "Circular Processing of Seawater Brines from Saltworks for Recovery of Valuable Raw Materials" (SEArcularMINE) project. The overall project objective aims to valorize the spent bitterns of ancient and still-used saltworks located in the Mediterranean Sea. The target is to extract minerals and produce on-site chemical reagents and energy embracing the circular economy approach. It has been reported that almost 10 million tonnes per year of sea salt is produced in the Mediterranean Sea alone, generating about 10 million m^3/year of exhausted bitterns. Considering an average Mg^{2+} content of 50 g/L, ~1.2 million tonnes of $Mg(OH)_2(s)$ can be produced covering 30% of the $Mg(OH)_2$ global demand [38]. Concerning the economics of the proposed approach, with a focus on $Mg(OH)_2$ production, only external electric energy would be required. Therefore, no reagent transport costs or NaOH pellets are foreseen. In the integrated SEArcularMINE scheme, NaOH solutions will be produced in loco by

adopting an EDBM (electrodialysis with a bipolar membrane) unit. Culcasi et al. [39] discussed the economics of NaOH production through EDBM, showing manufacturing costs in the same range as commercially available NaOH products. An EDBM unit is an energivorous unit, but it will also provide acids streams for the regeneration of selective adsorbent columns employed for the recovery of trace elements from bitterns. Note that EDBM units can be integrated into green power grids, e.g., wind or solar, thus drastically reducing $Mg(OH)_2$ production costs. Life-cycle assessments and economic feasibility analyses will be conducted in the SEArcularMINE project to better address the associated impacts and costs of the process.

The present work reports an extensive and detailed experimental campaign aimed at assessing MH recovery and purity from two bitterns collected from the Margi and Galia evaporation ponds of the Trapani saltworks (Sicily, Italy). Artificial bitterns were also prepared, mimicking the macro-element composition of the real ones, in order to study any possible influence of the real nature of the employed bitterns on the MH precipitation process. Margi bitterns had a Mg^{2+} concentration up to ~60 g/L, while Galia bitterns had concentrations ~24 g/L. Ca^{2+} was lower than 200 mg/L in both bitterns. MH was precipitated by employing stoichiometric and over-stoichiometric NaOH solutions. A 2 mm circular, cross-sectional T-mixer reactor was adopted to ensure fast mixing of the reactants, mimicking the conditions in large industrial stirred-tank crystallizers. For the first time, MH purity, produced from real Trapani bitterns, was thoroughly investigated analyzing (i) digested samples of MH through ion chromatography and inductively coupled plasma spectrometry techniques and (ii) MH powdered samples using SEM-EDS, thermogravimetric (TGA) and XRD analysis. The reported results are very promising in view of designing a process for bittern valorization, exploiting saline water in all its forms, and mitigating mineral ore consumption and its related environmental issues.

2. Materials and Methods

2.1. Experimental Set-Up

The precipitation of MH from real and artificial bitterns was studied by employing a simple experimental setup, as shown Figure 1. The set-up consisted of (i) a 2 mm diameter, circular, cross-sectional T-mixer, drilled into a polymethyl methacrylate, PMMA, block, (right upper part of Figure 1) and (ii) two gear pumps (FG200/FG300 series, TEOREMA Pump Technology®, Italy) controlled by a dedicated LabVIEW code. The T-mixer had two horizontal feed pipes 20 mm long that merged in a 40 mm long vertical channel, i.e., the mixing channel. The T-mixer was chosen as an effective laboratory-scale reactor to achieve a high reactant mixing degree in a short mixing time [40,41], thus guaranteeing a homogenized supersaturation level throughout the entire precipitation process.
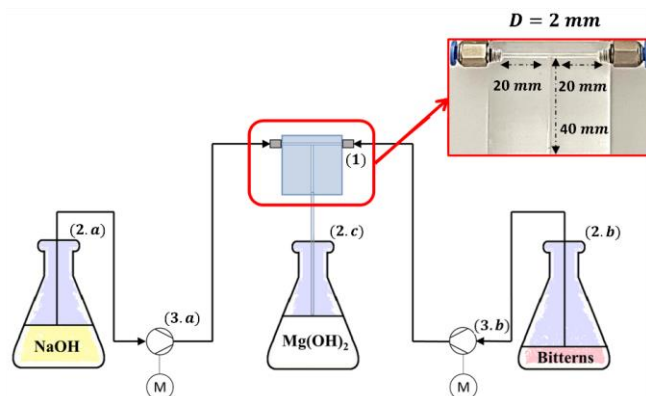

Figure 1. Schematic representation of the employed experimental set-up: (**1**) a 2 mm diameter circular, cross-sectional T-mixer; (**2.a**–**2.c**) beakers containing reactants, namely NaOH and bitterns, and produced $Mg(OH)_2$ suspensions; (**3.a**,**3.b**) gear pumps controlled by a dedicated LabVIEW code. In the (**upper right**), a picture of the employed T-mixer.

The main reaction occurring in the crystallizer is the precipitation of magnesium hydroxide that is described in the following equation:

$$Mg^{2+} + 2\,NaOH \;\rightarrow\; Mg(OH)_2\;(s) + 2\,Na^+ \tag{1}$$
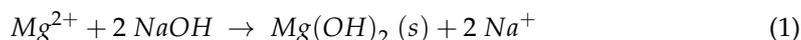
Real bitterns contain not only Mg^{2+} ions but also many other elements (e.g., Ca^{2+}, K^+, $B(OH)_4{}^-$, Br^-, $SO_4{}^{2-}$) or dissolved natural organic matter (DOM). Therefore, co-precipitation, inclusion or substitution of ions in the MH crystal structure or sorption onto the crystal faces of further compounds could also take place.

2.2. Solution Preparation and Compositions

The precipitation of MH from two different bitterns collected from the Margi and Galia saltworks, located in district of Trapani (Italy), was studied.

Two artificial bitterns were also prepared mimicking the macro-components contained in the real ones in order to better understand the influence of the real nature of the employed bitterns on the MH precipitation process. Specifically, similar concentrations of Na^+, K^+, Mg^{2+}, Ca^{2+} cations and Cl^-, $SO_4{}^{2-}$ ions were targeted. Artificial bitterns were prepared by dissolving KCl (Honeywell | Fluka™), NaCl (Volterra saltworks), $MgCl_2 \cdot 6H_2O$ (Geo-Green Snow Melter), Na_2SO_4 (Honeywell | Fluka™) and $CaCl_2$ (Honeywell | Fluka™) pellets.

Ion compositions in real and artificial bitterns were assessed using ion chromatography (IC), flame-atomic absorption spectroscopy (F-AAS), inductively coupled plasma optical emission spectrometry (ICP-OES) and inductively coupled plasma mass spectrometry (ICP-MS) techniques as discussed in Section 2.4. The bitterns' compositions are listed in Table 1.

Table 1. Ion composition of real and artificial bitterns adopted in the here-reported experimental campaign.

	Real Galia	Artificial Galia	Real Margi	Artificial Margi
Macro Components	**g/L**	**g/L**	**g/L**	**g/L**
Na	83.7 ± 0.5	82.2 ± 0.7	44.6 ± 1.6	38.0 ± 0.4
K	7.4 ± 0.3	7.7 ± 0.1	11.9 ± 2.6	14.8 ± 0.1
Mg	23.0 ± 4.4	24.0 ± 1.5	60.5 ± 0.5	65.4 ± 0.6
Cl	193 ± 6	179.5 ± 0.6	200 ± 14	176 ± 1
SO$_4$	35 ± 1	36.0 ± 0.6	83.0 ± 5.5	85.7 ± 0.2
Br	1.3 ± 0.2	-	2.5 ± 0.2	-
Micro Components	**mg/L**	**mg/L**	**mg/L**	**mg/L**
Ca	232 ± 40	270 ± 20	139 ± 32	112 ± 2
B	110 ± 22	18.7 ± 0.2	187 ± 8	46.6 ± 0.5

All MH precipitation tests were carried out using NaOH solutions prepared by dissolving NaOH pellets (Honeywell | Fluka™, with a purity of >98%) in deionized water. NaOH solution concentrations were checked via titration using a standard HCl solution.

2.3. Experimental Tests and Methodological Procedures

MH precipitation experiments were conducted to identify the best operating conditions for the complete recovery (i.e., >99.9%) of Mg^{2+} from bitterns producing high-purity MH powders. Two main operating parameters were investigated: (i) the flow-rate ratio between the NaOH and Mg^{2+}-containing solutions; and (ii) the hydroxyl/magnesium ion (OH^-/Mg^{2+}) ratio, with values corresponding to stoichiometric and 20% over-stoichiometric OH^-.

The flow-rate ratio (i) was preliminarily studied performing stoichiometric precipitation tests employing artificial solutions of $MgCl_2$ at Mg^{2+} concentration levels of 12.2 g/L (0.50 M) and 24 g/L (1.00 M). The NaOH/Mg^{2+}-solution flow-rate ratio was varied from 0.5 to 2.0 for the 0.50 M case and from 1.0 to 3.0 for the 1.00 M case. Note that artificial

MgCl$_2$ solutions were used only for the NaOH/Mg^{2+}-solution flow-rate assessment. Subsequently, the flow-rate ratio was investigated employing only Margi bitterns at selected NaOH/bittern flow-rate values of 2.0 and 3.0.

The hydroxyl/magnesium ion (OH$^-$/Mg^{2+}) ratio (ii) was studied performing stoichiometric and 20% over-stoichiometric OH$^-$ precipitation tests treating Margi and Galia bitterns with a NaOH/bittern flow-rate ratio value of 2.0. NaOH stoichiometric amounts were calculated based on an OH$^-$/Mg^{2+} molar ratio taking Equation (1) into account; e.g., if a 1.0 M Mg^{2+} solution is targeted, a 2.0 M NaOH solution would be prepared. In the NaOH solution preparation, Ca^{2+} precipitation was neglected, since its concentration is 100 times lower than that of Mg^{2+}.

All precipitation tests were carried out at room temperature. Table 2 lists all the operating details of the experimental tests.

Table 2. Operating conditions of experimental tests. The first 6 rows refer to precipitation tests performed using artificial MgCl$_2$ solutions. From row 7 to row 16, information regarding tests with real bitterns is listed. The first letter in the Tests column refers either to the Margi (M) or Galia (G) bitterns; (ii) the second letter specifies the nature of the bittern, i.e., real (R) or artificial (A); (iii) the third letter and numbers indicate stoichiometric (S) or 20% OH$^-$ excess (E) precipitation conditions and NaOH/bittern flow-rate ratios of 2.0 or 3.0.

Tests	Bittern Solution	OH$^-$/Mg^{2+}	Bittern Flow Rate (mL/min)	NaOH/Bittern Flow Rate Ratio	Mg^{2+} (M)	NaOH (M)
1M_S1			1160 ± 30	1.0		2.00 ± 0.04
1M_S2	Artificial MgCl$_2$	Stoichiometric	780 ± 20	2.0	1.00 ± 0.02	1.00 ± 0.02
1M_S3			547 ± 10	3.0		0.67 ± 0.01
0.5M_S0.5			1560 ± 40	0.5		2.00 ± 0.04
0.5M_S1	Artificial MgCl$_2$	Stoichiometric	1160 ± 30	1.0	0.50 ± 0.01	1.00 ± 0.02
0.5M_S2			780 ± 20	2.0		0.50 ± 0.01
M_R_S2			780 ± 20	2.0		2.50 ± 0.05
M_R_S3	Real Margi	Stoichiometric	547 ± 10	3.0	2.48 ± 0.05	1.70 ± 0.03
M_R_E2		20% excess OH$^-$	780 ± 20	2.0		3.00 ± 0.06
M_A_S2		Stoichiometric	780 ± 20	2.0		2.70 ± 0.05
M_A_S3	Artificial Margi		547 ± 10	3.0	2.69 ± 0.05	1.80 ± 0.03
M_A_E2		20% excess OH$^-$	780 ± 20	2.0		3.00 ± 0.06
G_R_S2		Stoichiometric	780 ± 20	2.0		1.00 ± 0.02
G_R_E2	Real Galia	20% excess OH$^-$	780 ± 20	2.0	0.96 ± 0.18	1.20 ± 0.03
G_A_S2		Stoichiometric	780 ± 20	2.0		1.00 ± 0.02
G_A_E2	Artificial Galia	20% excess OH$^-$	780 ± 20	2.0	0.97 ± 0.06	1.20 ± 0.03

Mg^{2+}-solutions and NaOH flow rates were calculated in order to achieve a total fluid flow rate of ~2340 mL/min in the vertical channel of the T-mixer (i.e., the mixing channel), resulting to a mean linear velocity of ~12.0 m/s. Under such flow conditions, short mixing times can be achieved leading to a good reactant homogenization [42].

After precipitation, MH suspensions were collected in glass beakers and the pH was measured within 30 s using a pH-meter WTW™ pH/Cond 3320. The suspension settled for 48 h and was then filtered using a Buchner funnel and 1.8 μm glass fiber filters (GE Healthcare Life Science Whatman™). The MH cake was washed using a deionized water volume at least equal to that of the filtered suspension. The cake was then dried at 105 °C in an oven for 24 h. Finally, solids were crushed using a mortar and pestle. Figure 2 shows a schematic representation of the adopted experimental procedure along with details of the employed techniques used for the Mg^{2+} recovery and purity assessment; see Section 2.4 for further details.
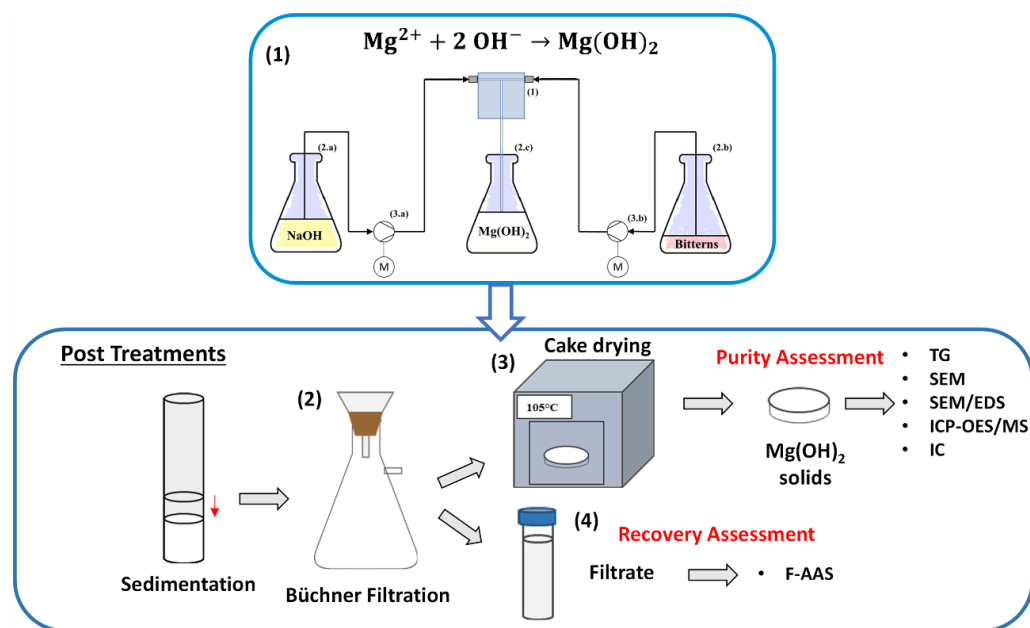
Figure 2. Adopted experimental procedure: (**1**) Mg(OH)$_2$(s) was produced using a 2 mm diameter circular, cross-sectional T-mixer; (**2**) suspensions were settled and filtered; (**3**) Mg(OH)$_2$(s) cake purity was analyzed via TG, SEM/EDS, ICP-OES/MS and IC techniques, while (**4**) the Mg(OH)$_2$(s) recovery was assessed by analyzing the total Mg^{2+} in the filtrate via the F-AAS technique.

2.4. Analytical Equipment and Procedures

Several analytical techniques were employed to assess bittern concentrations, Mg^{2+} recovery and the purity of produced MH solids.

1. Bittern concentration. Na$^+$, K$^+$, Mg^{2+}, Cl$^-$, SO$_4^{2-}$ and Br$^-$ ions were assessed through ion chromatography (IC, Metrohm 882 Compact IC plus and Dionex ICS-1000/1100, located at UNIPA and UPC laboratories); Ca^{2+} was measured via flame-atomic absorption spectroscopy (F-AAS, AAnalyst 200 PerkinElmer (Waltham, MA, USA) spectrometer, located at UNIPA) and inductively coupled plasma mass spectrometry (ICP-MS, 7800 ICP-MS from Agilent Technologies (Santa Clara, CA, USA), located at UPC) techniques; and B(III) was determined using inductively coupled plasma optical emission spectrometry (ICP-OES, Optima 2100 DV PerkinElmer (Green Bay, WI, USA) spectrometer, located at UNIPA) and the ICP-MS. Bittern samples were diluted in deionized water before measurement.
2. Mg^{2+} recovery (ion concentrations in filtrates, see Figure 2). Mg^{2+} and Ca^{2+} concentrations in the filtrates were measured using the F-AAS technique. Samples were diluted in deionized water before measurement. Samples were diluted and acidified with HNO$_3$ (Sigma–Aldrich, ≥65%, Saint Louis, MO, USA) to reach a pH of around 5 before measurement.
3. Mg(OH)$_2$ cationic purity (e.g., total content of cations in the precipitated MH). Approximately 100 mg of MH powder was dissolved in 1 M HCl (Honeywell | Fluka^{TM}). Mg^{2+}, Ca^{2+} and Na$^+$ concentrations were measured via IC at UNIPA laboratories. B(III) traces were also measured though ICP-OES. The same samples were also analyzed at UPC laboratories by dissolving 50 mg of MH in 100 mL of aqua regia and employing ICP-MS and an inductively coupled plasma optical emission spectrometer (5100 ICP-OES from Agilent Technologies, United States).
4. Mg(OH)$_2$ mass purity. The crystalline structure and impurities present in the Mg(OH)$_2$ powders were semi-quantitatively analyzed through an X-ray diffraction (XRD, Empyrean, Malvern PANalytical, United Kingdom, diffractometer, at UNIPA laboratories) technique using CuKa radiation (1.542° A, 40 KV, 40 mA) in the 2θ range of 10–70° at a step size of 0.05 and a step time of 144 s. The solids' purity was also

investigated via thermogravimetric analysis (TGA, STA 449 F1 Jupiter analyzer, NET-ZSCH, at UNIPA laboratories). TGA analyses were conducted at a heating rate of 10 °C/min from 30 °C to 1000 °C, under a constant nitrogen flow of 20 mL/min. The solids' mass purity and morphological shapes were further assessed via scanning electron microscopy (SEM FEI, United States, Quanta 200 FEG and JEOL, Japan, JSM-7001F equipment at UNIPA and UPC laboratories, respectively) and via elemental microanalysis adopting energy dispersive X-ray spectroscopy (EDS).

2.5. MH Precipitation Performance Parameters

The Mg^{2+} recovery and the produced MH-solids purity were assessed for each experimental test in order to identify the best operating conditions at which high Mg^{2+} recovery and high MH purity products can be achieved from bitterns.

The Mg^{2+} recovery was calculated as the difference between the initial and final mass of magnesium in the solution divided by the initial mass. The final solution volume was calculated as the sum of the volumes of the feed bitterns and the NaOH solution:

$$Mg\ recovery\ \% = \frac{C_{Mg2+,\ bittern} * V_{bittern} - C_{Mg2+,\ filtrate} * V_{final}}{C_{Mg2+,\ bittern} * V_{bittern}} \cdot 100 \tag{2}$$

The presence of Ca^{2+} ions can affect MH purity. Therefore, Ca^{2+} recovery was also calculated as it was for Mg^{2+}:

$$Ca\ recovery\ \% = \frac{C_{Ca2+,\ bittern} * V_{bittern} - C_{Ca2+,\ filtrate} * V_{final}}{C_{Ca2+,\ bittern} * V_{bittern}} \cdot 100 \tag{3}$$

$Mg(OH)_2$ purity was calculated as:

1. The ratio between the Mg^{2+} ion concentration (mg/g) in the dissolved solids with respect to all the other cations (cationic purity) detected through IC measurements:

$$Cationic\ purity = \frac{C_{Mg2+}}{\sum_{i=1}^{N} C_i} \cdot 100 \tag{4}$$

where N is the total number of cations and C_i (mg/g) is the concentration of the i-th cation.

2. The ratio between the $Mg(OH)_2$ mass ($m_{Mg(OH)2}^{\Delta T=320-480°C}$) associated with water-mass loss in a temperature range between 320 °C and 480 °C (see Section TG analysis for further details), measured using TG analysis, over the dry sample mass (mass purity). Note that the dry mass was calculated by subtracting the humidity content ($m_{H2O}^{\Delta T=30-200°C}$) determined in a temperature range between 30 °C and 200 °C to the total initial sample mass. Therefore, mass purity from TG analysis was calculated as:

$$Mass\ purity\ \% = \frac{m_{Mg(OH)2}^{\Delta T=320-480°C}}{m_{sample}^{Total} - m_{H2O}^{\Delta T=30-200°C}} * 100 \tag{5}$$

3. Results

The main objective of the present study was the assessment of the influence of two main operating parameters on Mg^{2+} recovery from bitterns and on precipitated MH purity, as detailed in the following Sections 3.1 and 3.2, respectively. In particular, the precipitation of MH from two real and artificial bitterns, namely Margi and Galia, was carried out by (i) varying the NaOH/bittern flow-rate ratio and (ii) performing stoichiometric and 20% OH^- over-stoichiometric tests; see Table 2.

3.1. Magnesium Recovery

3.1.1. Influence of the NaOH/Mg^{2+}-Solution Flow-Rate Ratio

The influence of the NaOH/Mg^{2+}-solution flow-rate ratio was investigated studying only stoichiometric Mg(OH)$_2$ precipitation tests. Stoichiometric tests were first carried out using Mg^{2+} 0.50 M and 1.00 M artificial MgCl$_2$ solutions. NaOH/Mg^{2+}-solution flow-rate ratios ranging from 0.5 to 2.0 and from 1.0 to 3.0 were adopted for the 0.50 M and 1.00 M artificial solutions, respectively.

Mg^{2+} concentration in the filtrates, recovery and pH values (measured after the precipitation) are shown in Figure 3. Note that, Mg^{2+} concentrations values are reported as the measured concentrations in the filtrates multiplied by the dilution factor occurring during the addition of NaOH solutions, e.g., a dilution factor of 2.0 or 3.0 is used when the NaOH/Mg^{2+}-solution flow-rate ratio is equal to 1.0 or 2.0.
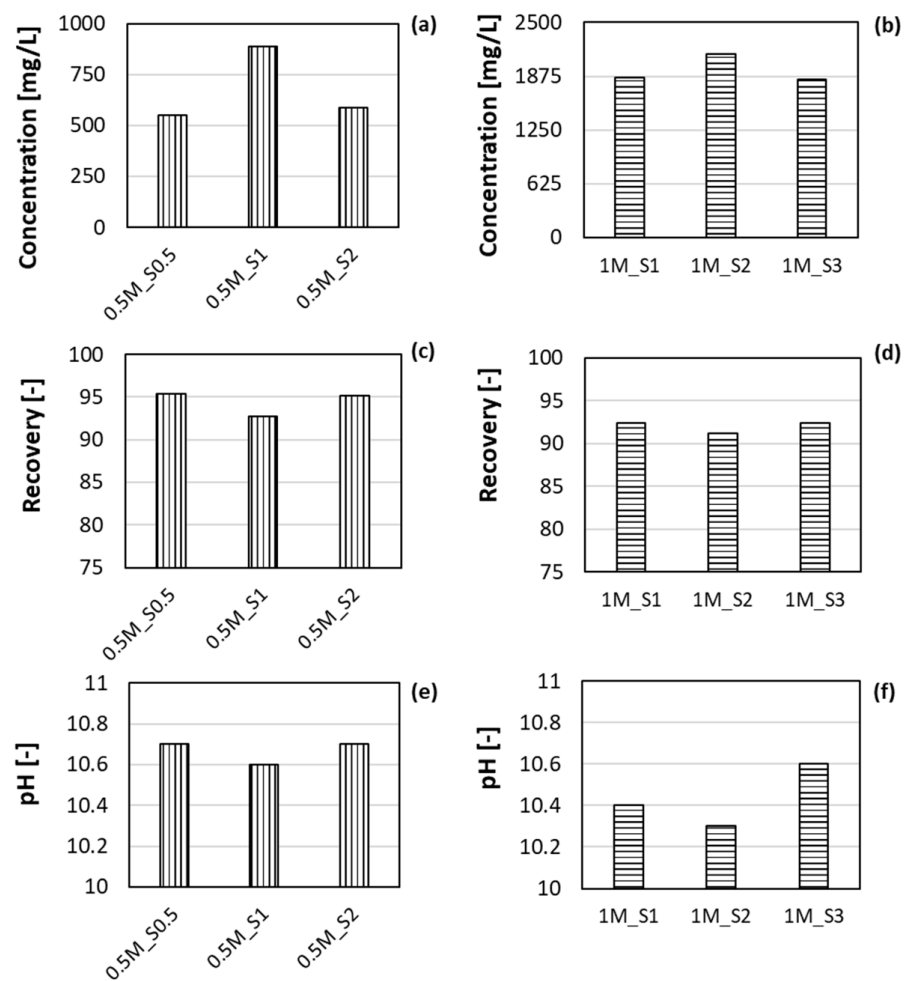

Figure 3. (**a**,**b**), Final Mg^{2+} concentrations in the filtrates; (**c**,**d**), Mg recovery; (**e**,**f**), pH values, for stoichiometric precipitation tests performed using Mg^{2+} 0.50 M (**a**,**c**,**e**) and 1.00 M (**b**,**d**,**f**) artificial MgCl$_2$ solutions at NaOH/Mg^{2+}-solution flow-rate ratios ranging from 0.5 to 2.0 and from 1.0 to 3.0, respectively.

In the case of artificial Mg^{2+} 0.50 M MgCl$_2$ solutions, final Mg^{2+} concentrations in the filtrates ranged between ~600 mg/L and ~900 mg/L (Figure 3a). Consequently, similar Mg^{2+} recovery values of ~93–95% were calculated for all the investigated NaOH/Mg^{2+}-solution flow-rate ratios (Figure 3c). The small Mg^{2+} concentration differences can be caused by either the use of stoichiometric MgCl$_2$ and NaOH solutions that are not exactly 100% or small fluid flow-rate unbalances that can lead to slightly different equimolar

precipitation conditions, as suggested by the small differences of the final suspension pH values; see Figure 3e.

A negligible influence of the NaOH/Mg^{2+}-solution flow-rate ratio on Mg^{2+} recovery is also observed for the precipitation cases performed with artificial Mg^{2+} 1.00 M MgCl$_2$ solutions. In this case, final Mg^{2+} concentration values in the filtrates range between ~1900 and ~2100 mg/L, as reported in Figure 3b, leading to similar Mg^{2+} recovery values of about ~92% for all the investigated NaOH/Mg^{2+}-solution flow-rate ratios (Figure 3d). For the sake of completeness, final suspension pH values after precipitation are reported in Figure 3f.

3.1.2. Influence of the NaOH/Bittern Flow Rate Ratio

Based on results of Section 3.1.1, only two NaOH/bittern flow-rate ratio values of 2.0 and 3.0 were investigated by preforming stoichiometric Mg(OH)$_2$ precipitation tests using real and artificial Margi bitterns. In this case, both Mg^{2+} and Ca^{2+} ions in the filtrates were studied.

Final Mg^{2+} and Ca^{2+} concentrations in the filtrates, recovery, and pH values (measured after the precipitation) are reported in Figure 4. Note that, also in this case, concentrations are reported taking into account the dilution factor occurring during the precipitation process (see Section 3.1.1).
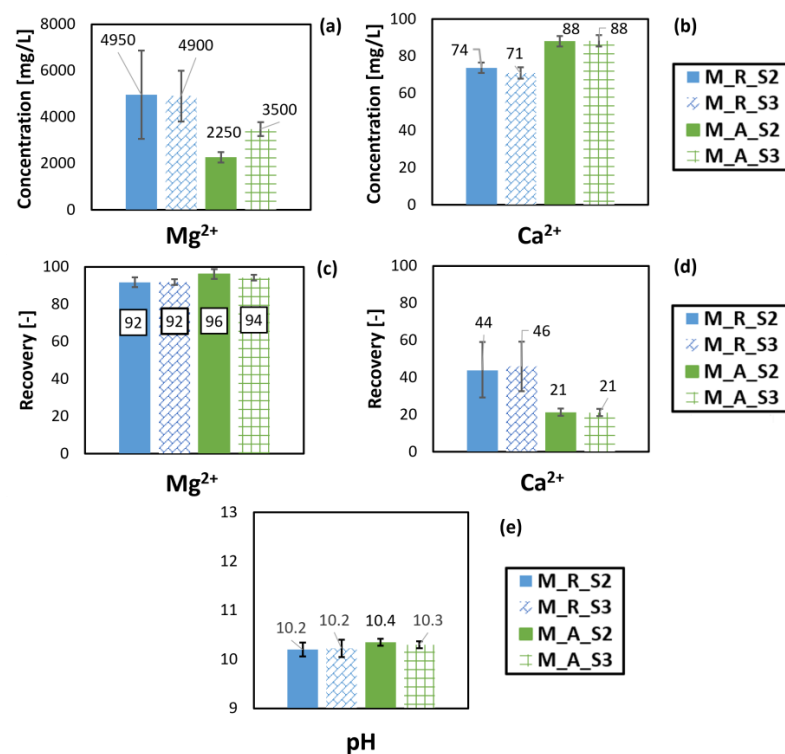

Figure 4. (**a**,**b**): Mg^{2+} and Ca^{2+} concentrations in the filtrates for Tests M_R_S2 and M_R_S3 (real Margi bitterns) and Tests M_A_S2 and M_A_S3 (artificial Margi bitterns) under stoichiometric Mg(OH)$_2$ precipitation conditions for NaOH/bittern flow-rate ratios equal to 2.0 and 3.0; (**c**,**d**): Mg^{2+} and Ca^{2+} recovery; (**e**): final measured pH values.

Comparable final Mg^{2+} concentrations of ~4900 mg/L were observed in the filtrates of real bitterns regardless of the employed NaOH/bittern flow-rate ratio; see Figure 4a. Lower final Mg^{2+} concentrations of ~2250 and 3500 mg/L were obtained in the filtrates in the case M_A_S2 and M_A_S3, respectively. The different final Mg^{2+} concentrations in the artificial bittern case can be associated with a final suspension pH value that is higher in the M_A_S2 sample than in the M_A_S3 sample, as shown in Figure 4e. Calcium concentrations of ~70 and ~88 mg/L were measured for real and artificial bitterns, respectively. Calcium

concentrations were influenced neither by the different NaOH/bittern flow-rate ratio nor by the final pH values; see Figure 4b.

Mg^{2+} recovery of ~92% was calculated from real bitterns, while recovery increased using artificial ones reaching values up to ~96% (Figure 4c). Ca^{2+} recovery was ~44% in the case of real bitterns, while it decreased down to ~20% in artificial ones (Figure 4d). These small recovery differences may be attributed to the different nature of the employed bitterns that contain many other chemical compounds which may interfere with $Mg(OH)_2$ precipitation. A detailed characterization of the minor and major elements in the bitterns of the Trapani saltworks was presented by Vicari et al. [43].

Overall, the results obtained using both artificial $MgCl_2$ solutions and bitterns do not show a significant Mg^{2+} recovery variation as a function of the $NaOH/Mg^{2+}$-solution flow-rate ratio. In addition, in all cases, the recovery never reached a 100% value. Based on the latter observation, only tests at a flow-rate ratio of 2.0 are discussed hereinafter.

The $NaOH/Mg^{2+}$-solution flow-rate results also highlight the possibility of using diluted NaOH solutions to treat highly concentrated Mg^{2+} solutions by adopting $NaOH/Mg^{2+}$-solution flow-rate ratios higher than 1.0 without affecting Mg^{2+} recovery. As an example, a 5.0 M NaOH solution would be required to treat Margi bitterns adopting a NaOH/bittern flow-rate ratio of 1.0; such a concentrated NaOH solution would be difficult to handle, while in adopting a NaOH/bittern flow-rate ratio of 2.0 or 3.0, a NaOH solution of 2.5 M and 1.7 M, respectively, would be needed.

3.1.3. Influence of the OH^-/Mg^{2+} Ratio

The influence of the OH^-/Mg^{2+} ratio on Mg^{2+} recovery was assessed performing $Mg(OH)_2$ precipitation tests for Margi and Galia bitterns under hydroxyl ions in stoichiometric and over-stoichiometric conditions. All tests were carried out setting the NaOH/bittern flow-rate ratio to the value of 2.0.

Margi Bittern

Figure 5 reports Mg^{2+} and Ca^{2+} concentrations in the filtrates, recovery and final pH values obtained by treating real and artificial Margi bitterns with OH^- stoichiometric (M_R_S2 and M_A_S2) and 20% over-stoichiometric amounts (M_R_E2 and M_A_E2). Again, as discussed in Section 3.1.1, concentration values in the filtrates were corrected in order to take dilution effects during the precipitation process into account.

In Figure 5, a strong effect of the over-stoichiometric NaOH amount is observed. Specifically, Mg^{2+} and Ca^{2+} concentrations decreased from their stoichiometric values of ~4950–2250 mg/L and ~74–88 mg/L, respectively, to values lower than 30 mg/L; see Figure 5a,b.

This result is somehow expected, since the OH^- excess ensures a total consumption of both Mg^{2+} and Ca^{2+} ions, as is also indicated by the final suspensions pH values (Figure 5e). The pH values, in fact, are higher than 12, showing a residual amount of hydroxyl ions in the suspensions.

Consequently, Mg^{2+} and Ca^{2+} recoveries reached values up to >99.99% (Figure 5c,d). In the case of over-stoichiometric NaOH solutions, Ca^{2+} concentration values were lower than their limit of quantification (LOQ). Recovery values higher than 92% are indicated in Figure 5d, although a >99.9% recovery can be assumed.

Galia Bittern

Mg^{2+} and Ca^{2+} concentrations in the filtrates, recovery and final pH values for $Mg(OH)_2$ precipitation tests treating real and artificial Galia bitterns under stoichiometric (G_R_S2 and G_A_S2) and 20% OH^- over-stoichiometric amounts (G_R_E2 and G_A_E2) are reported in Figure 6. Also in this case, concentrations take dilution effects during precipitation into account.
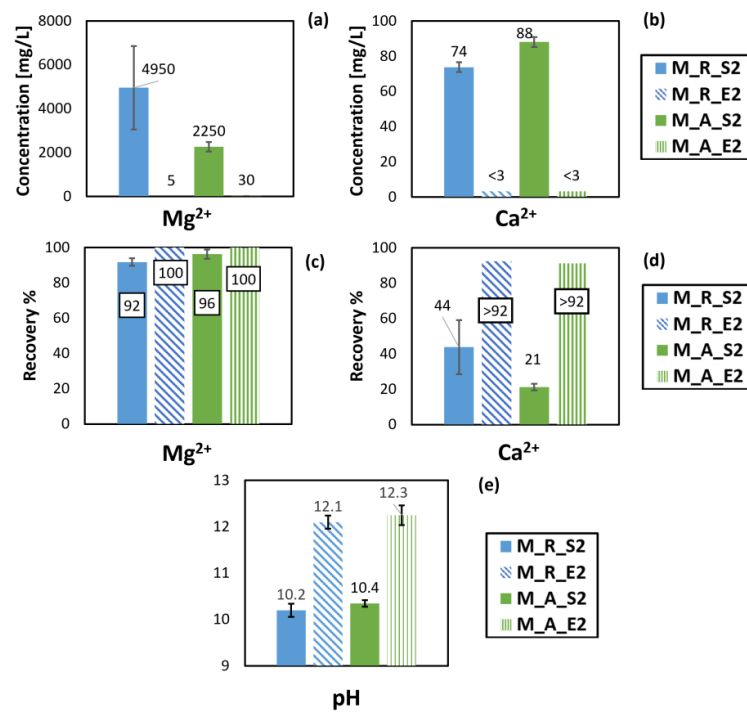
Figure 5. (**a**,**b**): Mg^{2+} and Ca^{2+} concentrations in the filtrates for $Mg(OH)_2$ precipitation tests using real and artificial Margi bitterns under stoichiometric (M_R_S2 and M_A_S2) and 20% OH^- over-stoichiometric (M_R_E2 and M_A_E2) conditions; (**c**,**d**): Mg^{2+} and Ca^{2+} recovery; (**e**): final measured pH values. Note that in some cases, Ca^{2+} concentration values were lower than their limit of quantification. All tests were carried out adopting a NaOH/bittern flow-rate ratio value of 2.0.

Figure 6. (**a**,**b**): Mg^{2+} and Ca^{2+} concentrations in the filtrates for $Mg(OH)_2$ precipitation tests using real and artificial Galia bitterns under stoichiometric (G_R_S2 and G_A_S2) and 20% OH^- over-stoichiometric (G_R_E2 and G_A_E2) conditions; (**c**,**d**): Mg^{2+} and Ca^{2+} recovery; (**e**): final pH values. In over-stoichiometric NaOH precipitation cases, Ca^{2+} concentrations were lower than their limit of quantification. All tests were carried out adopting a NaOH/bittern flow-rate ratio value of 2.0.
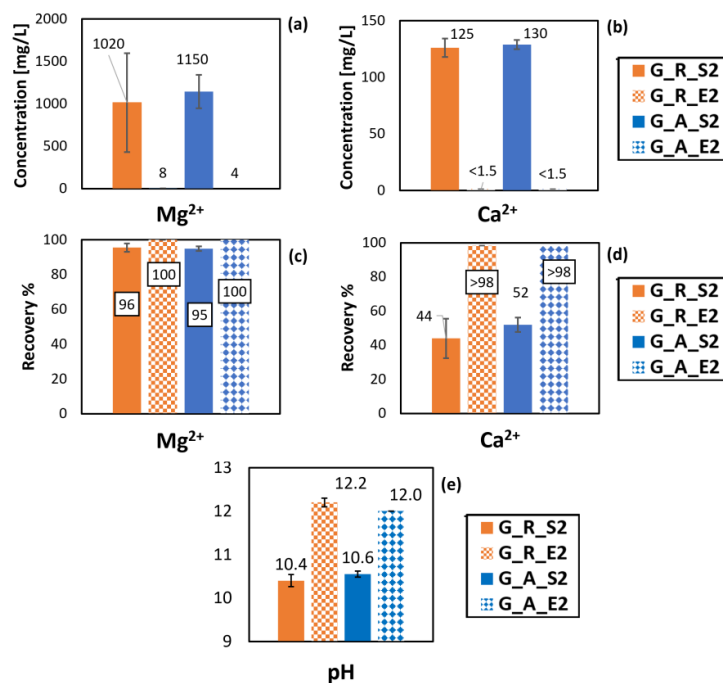
In Figure 6, similar final Mg^{2+} and Ca^{2+} concentration values of ~1020–1150 mg/L and ~125–130 mg/L in the cases G_R_S2 and G_A_S2, respectively, were obtained when performing stoichiometric precipitation tests using real and artificial bitterns (Figure 6a,b). Consequently, Mg^{2+} and Ca^{2+} recoveries are ~96–95% and ~44–52%, respectively; see Figure 6c,d. Such recovery values are close to those observed in the case of MH precipitation from Margi bitterns under stoichiometric conditions (Figure 4), where, in all cases, recovery did not reach a 100% value.

In addition, as also shown in the Margi bittern study, the strong effect of the NaOH excess can be seen in Figure 6. Mg^{2+} and Ca^{2+} concentrations diminished from their stoichiometric values to concentrations lower than 10 mg/L (Figure 6a,b). Therefore, Mg^{2+} and Ca^{2+} recoveries were >99.9% for both artificial and real bitterns. This is due to the OH^- excess that ensures a total consumption of Mg^{2+} and Ca^{2+} ions (final suspension pH values >12, Figure 6e).

Overall, results of the Margi (Figure 5) and Galia (Figure 6) precipitation tests confirmed that >99.9% Mg^{2+} recovery can be achieved from artificial and real bitterns employing over-stoichiometric NaOH solutions in accordance with data reported in the literature [13,21,25,36].

3.2. Mg(OH)$_2$ Purity Assessment

Cipollina et al. [36] have already demonstrated the possibility of achieving a >99.9% Mg recovery from saltwork bitterns. The authors also discussed the influence of several operating parameters on the cationic purity of produced MH particles, e.g., the influence of NaOH concentration and the volumetric flow rate in semi-batch systems. However, no information regarding solids mass purity was reported.

MH products must have a mass purity higher than 95% to be commercially attractive [26]. To better evaluate the possibility of producing high-mass-purity MH products from saltwork bitterns, thus turning waste into a valuable product, several analytical techniques were employed. In the following sections, first cationic purity is discussed; then attention is placed on solid mass purity.

3.2.1. Cationic Purity of MH

Cationic purity, understood as the presence of other cations than Mg^{2+}, was investigated by assessing cation concentrations in dissolved MH solids (see Section 2.4 for further details). The measured concentrations in the dissolved solids along with calculated cationic purity values, Equation (4), for Margi and Galia bitterns are reported in Table 3.

Table 3. Cation concentrations in dissolved Mg(OH)$_2$ solids assessed via IC analysis.

Tests	Ca (mg/g)	Mg (mg/g)	Na (mg/g)	Cationic Purity (%)
M_R_S2	<2.0 *	376.0 ± 0.6	1.82 ± 0.46	>99.0
M_R_E2	<2.0 *	375.0 ± 1.4	3.51 ± 0.03	>99.0
M_A_S2	<2.0 *	387.0 ± 0.8	<0.5 *	>99.0
M_A_E2	<2.0 *	385.0 ± 0.9	<0.5 *	>99.0
G_R_S2	<2.0 *	371.0 ± 3.4	2.49 ± 1.14	>99.0
G_R_E2	<2.0 *	376.0 ± 0.1	<0.5 *	>99.0
G_A_S2	<2.0 *	378.0 ± 0.3	3.20 ± 0.19	>99.0
G_A_E2	<2.0 *	382.0 ± 0.9	<0.5 *	>99.0

Note: * Concentrations lower than the limit of quantification.

From Table 3, Ca^{2+} concentration is always below its limit of quantification (LOQ), even for samples obtained under NaOH over-stoichiometric solutions. This result is due to a very low initial Ca^{2+} concentration in the bitterns that is 100 times lower than that for Mg^{2+}.

In same samples, traces of Na^+ are found. These traces can be mainly attributed to the need of a further cake-washing step, since some residuals of very soluble compounds, e.g., NaCl and Na_2SO_4, may be still present in the cake. For the sake of completeness, the M_R_S2 and M_R_E2 MH powders were further washed using ultrapure water. After washing, Na^+ concentrations were found to be lower than their limit of quantification, while Mg^{2+} concentrations increased up to 390.0 mg/g, thus confirming the assumed need for a better washing of the MH cakes during filtration to remove displacement of the brine from the surface of MH crystals.

Magnesium is the most abundant ion, and its cationic purity, calculated using Equation (4), is higher than ~99% in all cases regardless of the employed bittern or the operating conditions.

3.2.2. MH Mass Purity

Cationic purity was found to be very high (>99%); however, even very low concentrations of light elements, e.g., boron, can greatly affect mass purity, since light elements can precipitate production of high-weight compounds. B(III) is a light element forming a hydroxyl-acid type of species (e.g., H_3BO_3 and $H_2BO_3^-$) whose presence on the MH crystal structure could be more strongly associated with superficial sorption or occlusion phenomena than potential inclusion in the crystal structure substituting Mg^{2+} ions, as may happen with Ca^{2+}. In order to assess the MH samples, mass purity thermogravimetric (TG), X-ray and SEM-EDS analyses were conducted.

TG Analysis

Thermogravimetric (TG) analysis is a commonly employed technique for the study of a powder's mass purity. Thermogravimetry (TG) and derivative thermogravimetry (DTG) curves for MH powders produced from real Margi and real Galia bitterns are shown in Figure 7. The TG curves report the sample mass variations as functions of an imposed temperature change. The DTG curves plot the rate of change of mass with respect to temperature against temperature. In the latter case, downward and upward curves indicate endothermic and exothermic phenomena, respectively.

Three main weight losses can be identified in the TG curves:

1. The first weight loss, observed between 30 °C and 320 °C, is attributed to the mass sample loss due to residual humidity, free water and adsorbed water in the sample. In this temperature range also, water of crystallization can be lost by hydrate compounds, e.g., hydrate sulphates or borates. The mass loss in the temperature range between 30 °C and 200 °C, however, can be attributed to the samples' humidity [19,44]; therefore the mass losses in the 30 °C and 200 °C temperature range were subtracted from the total initial sample mass to determine the dry one.
2. The second major weight loss occurred in the temperature range between 320 °C and 480 °C. It is related to thermal decomposition of $Mg(OH)_2(s)$ and transformation onto $MgO(s)$ particles:

$$Mg(OH)_2(s) \rightarrow MgO(s) + H_2O(v)\ \Delta H_{298K} = 1300\ kJ\ kg^{-1} \tag{6}$$

In this thermal range, weight losses from 27.2% to 28.6% were measured. These values are lower than the theoretical one of 30.8% wt calculated on a dry mass base [45]. In fact, the former values increase up to 27.8% and 29.8%, respectively, if a dry mass sample is considered.

3. A further mass loss, between 480 °C and 1000 °C, was also noticed after $Mg(OH)_2$ decomposition. Ardizzone et al. [46] and Wang et al. [47] attributed this mass loss to the slow and continuous desorption of residual OH^- groups bonded to the $MgO(s)$ lattice. Ardizzone et al. [46] and Wang et al. [47] based their consideration on Fourier transform infrared spectroscopy studies that showed a strong $MgO(s)$ affinity towards the surface chemisorbed-OH groups. It should be noted that, if the mass loss would be correlated to further $Mg(OH)_2(s)$ decomposition, the final mass purities of the

samples would increase. Therefore, the here-reported mass purity values are likely to be an underestimation of the actual $Mg(OH)_2(s)$ powder's purity.
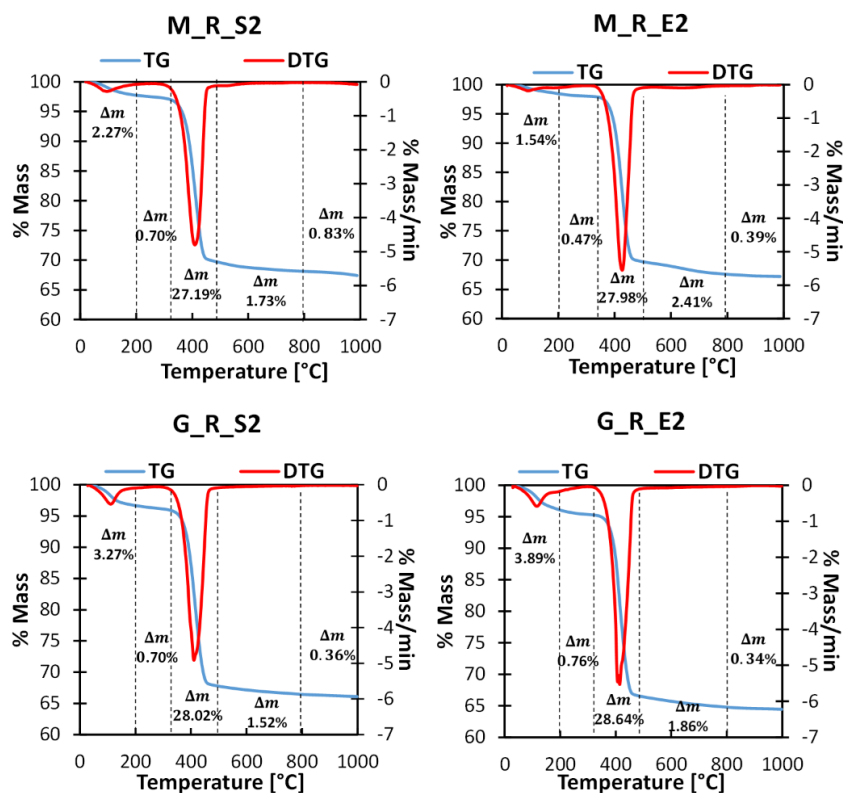

Figure 7. Thermogravimetric (TG) and derivative thermogravimetric curves (DTG) of $Mg(OH)_2$ solids precipitated from real Margi and real Galia bitterns under stoichiometric (M_R_S2 and G_R_S2) and over-stoichiometric (M_R_E2 and G_R_E2) NaOH solution conditions.

MH mass purities calculated using Equation (5) are reported in Figure 8 both for artificial and real Margi and Galia bitterns.
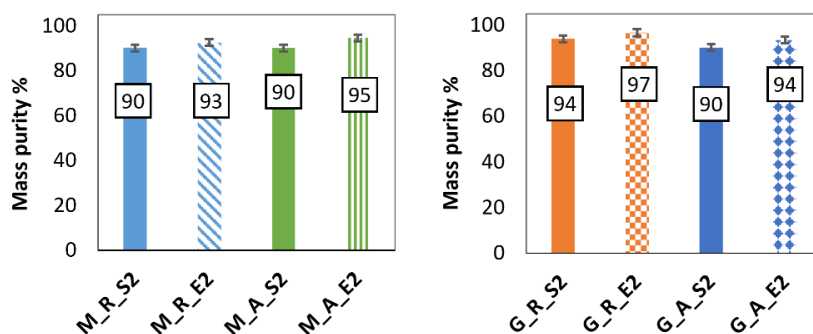

Figure 8. $Mg(OH)_2$ mass purities calculated using Equation (5) from TG curves for real and artificial Margi and Galia bitterns under stoichiometric and over-stoichiometric NaOH solution conditions.

From Figure 8, very high MH mass purity values (>90%) can be observed. Interestingly, solids produced using over-stoichiometric NaOH solutions show higher purity values with respect to samples precipitated in stoichiometric conditions, reaching values up to ~97% for the G_R_E2 sample, a value complying with market requirements.

To further understand this trend, boron concentration in the solids was assessed (see Section 2.4), as reported in Table 4.

As reported in Table 4, boron traces are higher in solids precipitated under stoichiometric NaOH conditions with respect to those obtained at over-stoichiometric conditions. Boron concentration decreases from ~1.71 mg/g to ~0.90 mg/g in M_R_S2 and M_R_E2 samples, or from ~1.40 mg/g in the G_R_S2 samples to a concentration lower than its limit of quantification in the G_R_E2 samples. The different boron concentration is attributed to the different value of pH at the end of the precipitation process. At pH values higher than 12, it has been described that the adsorption of borate ions onto the surface of magnesium hydroxide is hindered; thus, lower boron is entrained in MH solids [32]. The latter consideration explains the mass purity trend shown in Figure 8.

Table 4. Boron concentration in dissolved solids obtained employing ICP-OES and IPC-MS techniques.

Tests	B (mg/g)
M_R_S2	1.71 ± 0.18
M_R_E2	0.91 ± 0.33
M_A_S2	0.81 ± 0.21
M_A_E2	0.38 ± 0.08
G_R_S2	1.40 ± 0.05
G_R_E2	<0.3 *
G_A_S2	0.45 ± 0.03
G_A_E2	<0.3 *

Note: * Concentrations lower than the limit of quantification.

For the sake of completeness, the $Mg(OH)_2$ solid mass purity values of samples produced from real Margi bitterns under stoichiometric and over-stoichiometric conditions adopting NaOH/bittern flow rate ratios of 2.0 and 3.0 are reported in Figure 9.
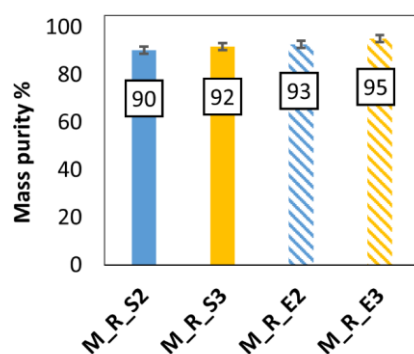

Figure 9. $Mg(OH)_2$ mass purity calculated using Equation (5) from TG curves for $Mg(OH)_2$ solids precipitated from Margi bitterns under stoichiometric and 20% OH^- over-stoichiometric conditions adopting NaOH/bittern flow-rate ratios of 2.0 and 3.0.

Comparable mass purity values were obtained by adopting different NaOH/bittern flow-rate ratios. Mass purity values were 2% higher in samples produced at a NaOH/bittern flow-rate ratio of 3. Such low differences can be attributed to measurement errors or the slightly higher or lower presence of soluble impurities in the samples rather than to an effective influence of the NaOH/bittern flow-rate ratio. In addition, the same mass purity trend as the function of precipitation conditions, shown in Figure 8, was observed, namely mass purity always increases from 90–92% to 93–95% in OH^- over-stoichiometric tests.

Overall, traces of boron base compounds ($H_2BO_3^-$) and magnesium carbonates ($MgCO_3$), due to the aqueous precipitation system, are the expected species hindering the $Mg(OH)_2$ mass purity (values lower than 100%) [48] that, however, achieve very high values thanks to the low Ca^{2+} concentrations in the bitterns. The formation of Mg-borates

has been described in the literature; however, the values of the total concentration of B in the bitterns are too far away to justify the precipitation of those mineral phases.

Mineralogical Characterization of MH Samples Using XRD

The XRD patterns of MH solids produced from real Margi bitterns under NaOH stoichiometric precipitation conditions (M_R_S2) and adopting 20% OH$^-$ excess (M_R_E2) are shown Figure 10a,b, respectively.
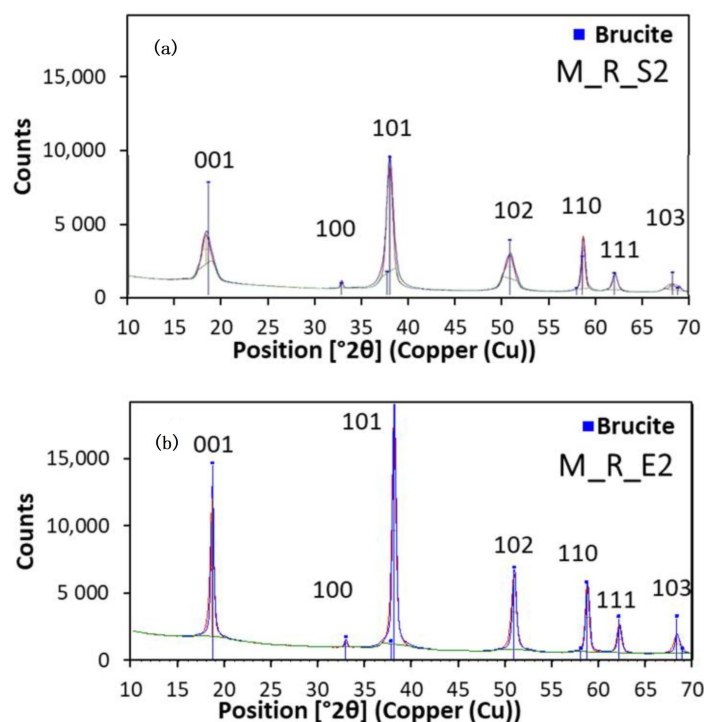

Figure 10. XRD patterns of Mg(OH)$_2$ solids produced from real Margi bitterns under NaOH stoichiometric precipitation conditions (M_R_S2), (**a**), and adopting an 20% OH$^-$ excess (M_R_E2), (**b**).

All XRD patterns exhibit typical diffraction peaks that are assigned to planes of the brucite crystalline form of Mg(OH)$_2$ (JCPDS 7-239) [44,49]. No extra diffraction peaks from impurities were identified in the XRD spectra (e.g., all of them are below 1%), thus indicating high MH purity and a high degree of crystallinity. No extra diffraction peaks were identified in the XRD spectra of all other MH precipitation tests (see Table 2); thus, for the sake of brevity, results are here omitted.

In Figure 10, it can also be noted that the XRD peaks' diffraction intensity and sharpness increase from samples produced under stoichiometric conditions (M_R_S2, Figure 10a) to those precipitated using a 20% OH$^-$ excess (M_R_E2, Figure 10b), thus indicating a higher crystallinity degree for solids produced using NaOH excess [50].

Morphological and Chemical Characterization of the MH Solids Using SEM-EDS

SEM-EDS analysis can provide information regarding particle shapes and local semi-quantitative chemical composition analysis using EDS. Figure 11 shows SEM-EDS results, relevant to Mg(OH)$_2$ samples, precipitated from real Margi bitterns using stoichiometric (M_R_S2) and over-stoichiometric NaOH solutions (M_R_E2).

Mg and O elements are the predominant ones associated with brucite. Traces lower than 0.5% wt of Na, Al, Si, S and Cl are also found. The presence of Na, Cl, and S traces can be due to either (i) a limited washing stage of the samples to displace the reacting bittern or (ii) entrained crystals during the filtration and solid drying processes. Si presence at trace levels can be attributed to the use of glass fiber filters, while carbon is mainly correlated to the use of carbon tape adopted to ensure solid attachment on SEM stubs. Other SEM

images, at higher magnifications of 3000 ×, 24,000× and 80,000/100,000×, for the same Margi solid samples M_R_S2 and M_R_E2 are shown in Figure 12, along with local EDS micro-analysis.

Processing option: All elements analysed (Normalised)

Spectrum	In stats.	C	O	Mg	Al	Si	S	Cl	Total
Spectrum 1	Yes	5.21	60.96	33.29	0.01	0.09	0.30	0.15	100.00
Spectrum 2	Yes	9.93	62.51	27.29		0.02	0.16	0.08	100.00
Spectrum 3	Yes	18.28	56.28	25.07		0.03	0.25	0.10	100.00
Spectrum 4	Yes	6.53	62.32	30.69	0.01	0.09	0.26	0.11	100.00
Max.		18.28	62.51	33.29	0.01	0.09	0.30	0.15	
Min.		5.21	56.28	25.07	0.01	0.02	0.16	0.08	

All results in weight%

M_R_S2

Processing option: All elements analysed (Normalised)

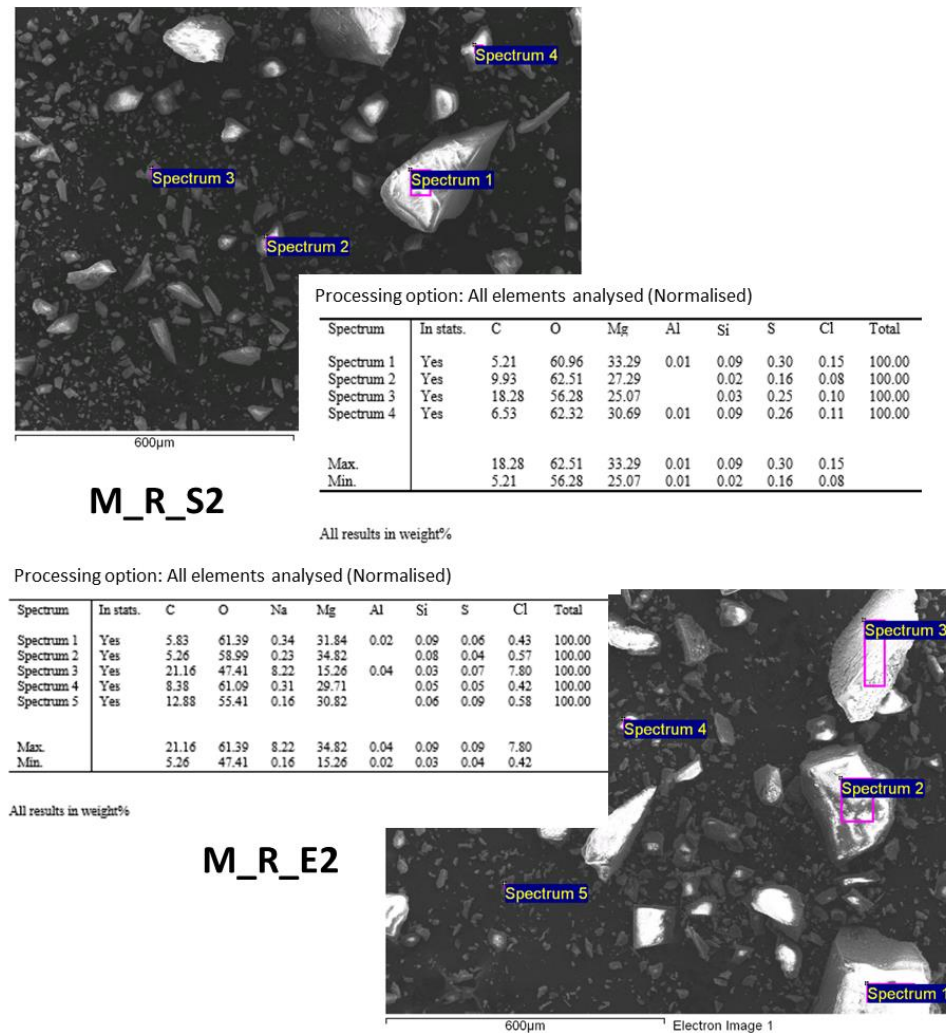| Spectrum	In stats.	C	O	Na	Mg	Al	Si	S	Cl	Total
Spectrum 1	Yes	5.83	61.39	0.34	31.84	0.02	0.09	0.06	0.43	100.00
Spectrum 2	Yes	5.26	58.99	0.23	34.82		0.08	0.04	0.57	100.00
Spectrum 3	Yes	21.16	47.41	8.22	15.26	0.04	0.03	0.07	7.80	100.00
Spectrum 4	Yes	8.38	61.09	0.31	29.71		0.05	0.05	0.42	100.00
Spectrum 5	Yes	12.88	55.41	0.16	30.82		0.06	0.09	0.58	100.00
Max.		21.16	61.39	8.22	34.82	0.04	0.09	0.09	7.80	
Min.		5.26	47.41	0.16	15.26	0.02	0.03	0.04	0.42	

All results in weight%

M_R_E2

Figure 11. SEM-EDS analysis of Mg(OH)$_2$ samples produced from real Margi bittern using stoichiometric (M_R_S2) and over-stoichiometric NaOH solutions (M_R_E2). Images were collected at PUPC laboratories.

In Figure 12, globular brucite shapes can be observed in M_R_S2 and M_R_E2 samples. The globular shape is the typical one reported when brucite is precipitated using a NaOH solution [51]. Interestingly, SEM images of the sample M_R_E2 also showed the co-presence of sand-rose/lamellar-like structures. Lamellar-like brucite shapes have been reported in precipitation cases adopting ammonia [51], but rarely for samples precipitated from NaOH solutions. The sand-rose structures can probably be attributed to the co-presence of many other ions in the real bittern influencing the nucleation and growth processes of precipitated brucite particles.

EDS micro-analysis showed no impurities, as only Mg and O elements were detected. The carbon (C) and gold (Au) element traces can be attributed to the use of carbon tape for sample attachment on the SEM stub and the initial spattering of a thin gold layer to better visualize the brucite structures at high magnifications, since brucite is a non-conductive material. For the sake of brevity, no other SEM images were reported as similar results as those of the M_R_S2 samples were obtained. Note that the sand-rose/lamellar shapes of sample M_R_E2 were not observed in the Galia bitterns even for samples produced at the

NaOH over-stoichiometric amount, probably due to the different chemical composition of the bitterns.
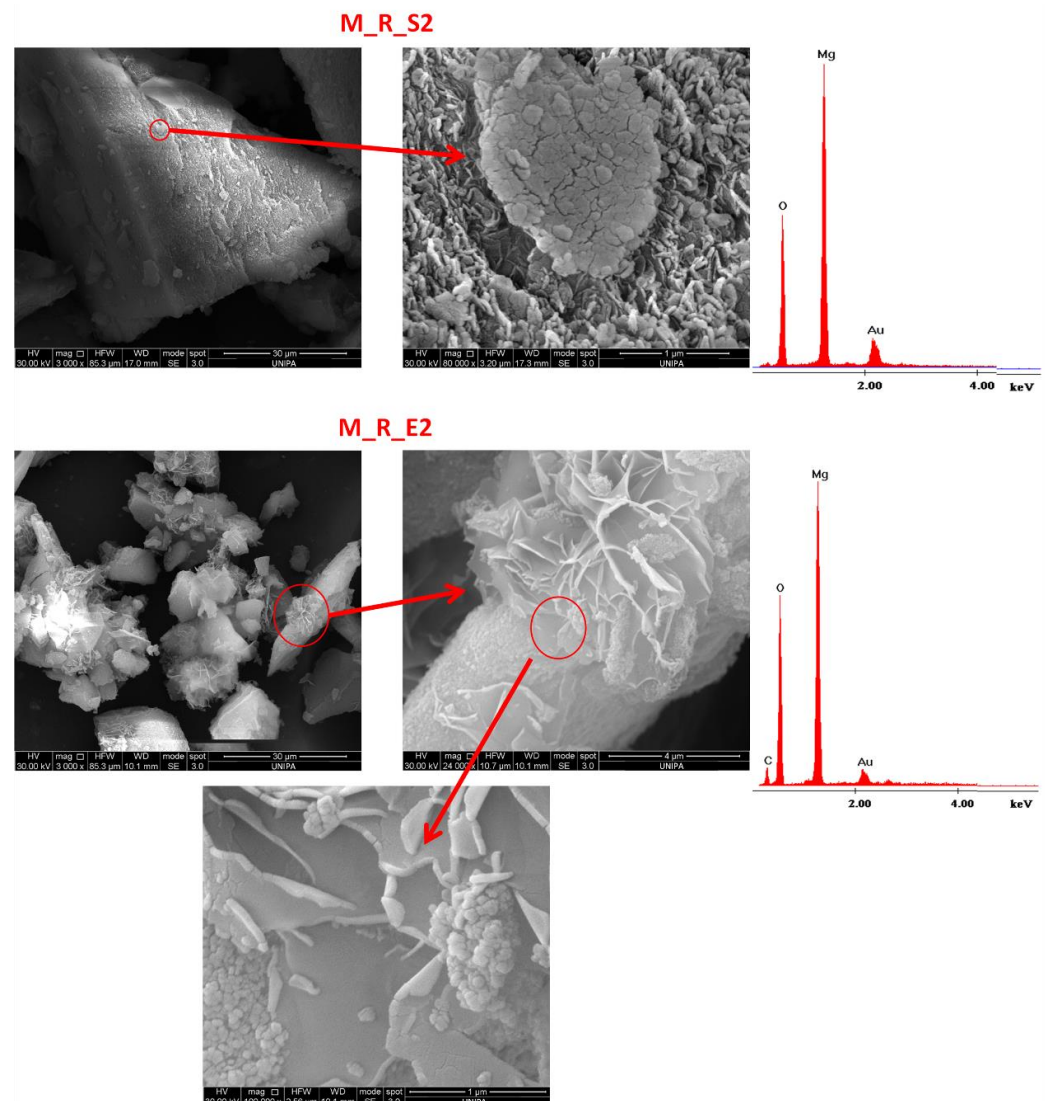

Figure 12. SEM-EDS micro-analysis of $Mg(OH)_2$ samples produced from real Margi bitterns using stoichiometric (M_R_S2) and over-stoichiometric NaOH solutions (M_R_E2) at magnifications of $3000\times$, $24,000\times$ and $80,000/100,000\times$. Images were obtained at UNIPA laboratories. The peak of Au is associated to the sample treatment to improve the quality of the images.

4. Conclusions

The recovery of Mg^{2+} from exhausted bitterns, the by-products of the sea-salt production process, was investigated with special attention on the purity of the precipitated $Mg(OH)_2$, to assess its potential application in the market.

The reactive crystallization method made use of NaOH solutions to precipitate Mg^{2+} in the form of $Mg(OH)_2$ from two bitterns collected from Margi and Galia final evaporation ponds of the Trapani saltworks (Italy).

A 2 mm diameter circular, cross-sectional, T-shaped mixer was employed to ensure fast mixing of the reactants. The influence of reactant flow-rate ratios and the OH^-/Mg^{2+} ratio was investigated. Experiments were also carried out using artificial bitterns mimicking the composition of the macro-compounds of real bitterns to better study the precipitation process.

The reactant flow rate ratios did not affect the Mg^{2+} recovery, as similar final ion concentrations in the filtrates were measured. On the other hand, as expected, the use of 20% over-stoichiometric NaOH solutions allowed the total recovery of Mg^{2+} ions.

As far as the Mg(OH)$_2$ powder's purity is concerned, cationic purity of >~99% was obtained regardless the employed bitterns or the operating conditions, while mass purity between 90% and 96% was measured. XRD analysis confirmed the presence of brucite with a high value of MH purity, since no other peaks associated with impurity traces were reported.

Overall, thanks to the low calcium concentration in the bitterns, it is feasible to use an excess of OH$^-$ ions for the precipitation of brucite from bitterns. The final high pH environment reduces boron adsorption on the precipitated brucite particles, thus ensuring a very pure product (mass purity >96%). The here-reported findings mark the actual possibility of producing high-purity brucite powders from waste saltwork bitterns complying with industrial requirements, thus making the bitterns sustainable alternative Mg^{2+} sources.

Author Contributions: G.B.: conceptualization, methodology, formal analysis, data curation, validation, investigation, writing—original draft, visualization; M.A.D.: methodology, formal analysis, data curation, validation, investigation, writing—review and editing, visualization; R.L.B.: data curation, investigation; J.L.R.: data curation, investigation, formal analysis; M.F.d.L.: data curation, investigation, formal analysis; J.L.C.: data curation, investigation, formal analysis, conceptualization, resources, supervision; A.P.: conceptualization, resources, supervision; A.C.: conceptualization, methodology, writing—review and editing, supervision, project administration, funding acquisition; A.T.: methodology, formal analysis, resources, supervision; G.M.: conceptualization, resources, supervision, writing—review and editing, project administration, funding acquisition. All authors have read and agreed to the published version of the manuscript.

Data Availability Statement: Data is available on Zenodo.

Conflicts of Interest: The authors declare no conflict of interest.

References

1. Bassioni, G.; Farid, R.; Mohamed, M.; Hammouda, R.M.; Kühn, F.E. Effect of Different Parameters on Caustic Magnesia Hydration and Magnesium Hydroxide Rheology: A Review. *Mater. Adv.* **2021**, *2*, 6519–6531. [CrossRef]
2. Gao, Y.; Wang, H.; Su, Y.L.; Shen, Q.; Wang, D. Influence of Magnesium Source on the Crystallization Behaviors of Magnesium Hydroxide. *J. Cryst. Growth* **2008**, *310*, 3771–3778. [CrossRef]
3. Deng, Y.; Li, X.; Ni, F.; Liu, Q.; Yang, Y.; Wang, M.; Ao, T.; Chen, W. Synthesis of Magnesium Modified Biochar for Removing Copper, Lead and Cadmium in Single and Binary Systems from Aqueous Solutions: Adsorption Mechanism. *Water* **2021**, *13*, 599. [CrossRef]
4. Pilarska, A.A.; Klapiszewski, Ł.; Jesionowski, T. Recent Development in the Synthesis, Modification and Application of Mg(OH)$_2$ and MgO: A Review. *Powder Technol.* **2017**, *319*, 373–407. [CrossRef]
5. Balducci, G.; Bravo Diaz, L.; Gregory, D.H. Recent Progress in the Synthesis of Nanostructured Magnesium Hydroxide. *CrystEngComm* **2017**, *19*, 6067–6084. [CrossRef]
6. Szymoniak, L.; Claveau-Mallet, D.; Haddad, M.; Barbeau, B. Application of Magnesium Oxide Media for Remineralization and Removal of Divalent Metals in Drinking Water Treatment: A Review. *Water* **2022**, *14*, 633. [CrossRef]
7. Luong, V.T.; Amal, R.; Scott, J.A.; Ehrenberger, S.; Tran, T. A Comparison of Carbon Footprints of Magnesium Oxide and Magnesium Hydroxide Produced from Conventional Processes. *J. Clean. Prod.* **2018**, *202*, 1035–1044. [CrossRef]
8. Bhatti, A.S.; Dollimore, D.; Dyer, A. Magnesia from Seawater: A Review. *Clay Miner.* **1984**, *19*, 865–875. [CrossRef]
9. Jakić, J.; Labor, M.; Martinac, V. Characterization of Dolomitic Lime as the Base Reagent for Precipitation of Mg(OH)$_2$ from Seawater. *Chem. Biochem. Eng. Q.* **2016**, *30*, 373–379. [CrossRef]
10. Turek, M.; Gnot, W. Precipitation of Magnesium Hydroxide from Brine. *Ind. Eng. Chem. Res.* **1995**, *34*, 244–250. [CrossRef]
11. Pramanik, B.K.; Shu, L.; Jegatheesan, V. A Review of the Management and Treatment of Brine Solutions. *Environ. Sci. Water Res. Technol.* **2017**, *3*, 625–658. [CrossRef]
12. Gao, L.; Yoshikawa, S.; Iseri, Y.; Fujimori, S.; Kanae, S. An Economic Assessment of the Global Potential for Seawater Desalination to 2050. *Water* **2017**, *9*, 763. [CrossRef]
13. Lee, C.H.; Chen, P.H.; Chen, W.S. Recovery of Alkaline Earth Metals from Desalination Brine for Carbon Capture and Sodium Removal. *Water* **2021**, *13*, 3463. [CrossRef]

14. An, J.W.; Kang, D.J.; Tran, K.T.; Kim, M.J.; Lim, T.; Tran, T. Recovery of Lithium from Uyuni Salar Brine. *Hydrometallurgy* **2012**, *117–118*, 64–70. [CrossRef]

15. Bonin, L.; Deduytsche, D.; Wolthers, M.; Flexer, V.; Rabaey, K. Boron Extraction Using Selective Ion Exchange Resins Enables Effective Magnesium Recovery from Lithium Rich Brines with Minimal Lithium Loss. *Sep. Purif. Technol.* **2021**, *275*, 119177. [CrossRef]

16. Zhang, X.; Zhao, W.; Zhang, Y.; Jegatheesan, V. A Review of Resource Recovery from Seawater Desalination Brine. *Rev. Environ. Sci. Biotechnol.* **2021**, *20*, 333–361. [CrossRef]

17. Shaddel, S.; Grini, T.; Andreassen, J.P.; Østerhus, S.W.; Ucar, S. Crystallization Kinetics and Growth of Struvite Crystals by Seawater versus Magnesium Chloride as Magnesium Source: Towards Enhancing Sustainability and Economics of Struvite Crystallization. *Chemosphere* **2020**, *256*, 126968. [CrossRef] [PubMed]

18. Chrispim, M.C.; de Souza, F.; Scholz, M.; Nolasco, M.A. A Framework for Sustainable Planning and Decision-Making on Resource Recovery from Wastewater: Showcase for São Paulo Megacity. *Water* **2020**, *12*, 3466. [CrossRef]

19. Kim, M.J.; Kim, S.; Shin, S.; Kim, G. Production of High-Purity MgSO4 from Seawater Desalination Brine. *Desalination* **2021**, *518*, 115288. [CrossRef]

20. Yousefi, S.; Ghasemi, B.; Tajally, M.; Asghari, A. Optical Properties of MgO and Mg(OH)$_2$ Nanostructures Synthesized by a Chemical Precipitation Method Using Impure Brine. *J. Alloys Compd.* **2017**, *711*, 521–529. [CrossRef]

21. Dong, H.; Unluer, C.; Yang, E.H.; Al-Tabbaa, A. Recovery of Reactive MgO from Reject Brine via the Addition of NaOH. *Desalination* **2018**, *429*, 88–95. [CrossRef]

22. Sano, Y.; Hao, Y.; Kuwahara, F. Development of an Electrolysis Based System to Continuously Recover Magnesium from Seawater. *Heliyon* **2018**, *4*, 923. [CrossRef]

23. Lalia, B.S.; Khalil, A.; Hashaikeh, R. Selective Electrochemical Separation and Recovery of Calcium and Magnesium from Brine. *Sep. Purif. Technol.* **2021**, *264*, 118416. [CrossRef]

24. Yu, X.; Cui, J.; Liu, C.; Yuan, F.; Guo, Y.; Deng, T. Separation of Magnesium from High Mg/Li Ratio Brine by Extraction with an Organic System Containing Ionic Liquid. *Chem. Eng. Sci.* **2021**, *229*, 116019. [CrossRef]

25. Casas, S.; Aladjem, C.; Larrotcha, E.; Gibert, O.; Valderrama, C.; Cortina, J.L. Valorisation of Ca and Mg By-Products from Mining and Seawater Desalination Brines for Water Treatment Applications. *J. Chem. Technol. Biotechnol.* **2014**, *89*, 872–883. [CrossRef]

26. Gong, M.H.; Johns, M.; Fridjonsson, E.; Heckley, P. Magnesium Recovery from Desalination Brine. In Proceedings of the CEED Seminar Proceedings, Bali, Indonesia, 17–18 November 2018; pp. 49–54.

27. Vassallo, F.; La Corte, D.; Cancilla, N.; Tamburini, A.; Bevacqua, M.; Cipollina, A.; Micale, G. A Pilot-Plant for the Selective Recovery of Magnesium and Calcium from Waste Brines. *Desalination* **2021**, *517*, 115231. [CrossRef]

28. Morgante, C.; Vassallo, F.; Battaglia, G.; Cipollina, A.; Vicari, F.; Tamburini, A.; Micale, G. Influence of Operational Strategies for the Recovery of Magnesium Hydroxide from Brines at a Pilot Scale. *Ind. Eng. Chem. Res.* **2022**, *61*, 15355–15368. [CrossRef]

29. La Corte, D.; Vassallo, F.; Cipollina, A.; Turek, M.; Tamburini, A.; Micale, G. A Novel Ionic Exchange Membrane Crystallizer to Recover Magnesium Hydroxide from Seawater and Industrial Brines. *Membranes.* **2020**, *10*, 303. [CrossRef]

30. Vassallo, F.; Morgante, C.; Battaglia, G.; La Corte, D.; Micari, M.; Cipollina, A.; Tamburini, A.; Micale, G. A Simulation Tool for Ion Exchange Membrane Crystallization of Magnesium Hydroxide from Waste Brine. *Chem. Eng. Res. Des.* **2021**, *173*, 193–205. [CrossRef]

31. Yousefi, S.; Ghasemi, B.; Tajally, M. PEG-Assisted Synthesis and Formation Mechanism of Mg(OH)$_2$ Nanostructures Using Natural Brine. *Appl. Phys. A Mater. Sci. Process.* **2020**, *126*, 641. [CrossRef]

32. Shand, M.A. *The Chemistry and Technology of Magnesia*; Wiley-Interscience: Hoboken, NJ, USA, 2006; ISBN 0471656038.

33. Fontana, D.; Forte, F.; Pietrantonio, M.; Pucciarmati, S.; Marcoaldi, C. Magnesium Recovery from Seawater Desalination Brines: A Technical Review. *Environ. Dev. Sustain.* **2022**. [CrossRef]

34. Lee, S.I.; Weon, S.Y.; Lee, C.W.; Koopman, B. Removal of Nitrogen and Phosphate from Wastewater by Addition of Bittern. *Chemosphere* **2003**, *51*, 265–271. [CrossRef] [PubMed]

35. Alamdari, A.; Rahimpour, R.M.; Esfandiari, N.; Nourafkan, E. Kinetics of Magnesium Hydroxide Precipitation from Sea Bittern. *Chem. Eng. Process. Process Intensif.* **2008**, *47*, 215–221. [CrossRef]

36. Cipollina, A.; Bevacqua, M.; Dolcimascolo, P.; Tamburini, A.; Brucato, A.; Glade, H.; Buether, L.; Micale, G. Reactive Crystallisation Process for Magnesium Recovery from Concentrated Brines. *Desalin. Water Treat.* **2015**, *55*, 2377–2388. [CrossRef]

37. Loganathan, P.; Naidu, G.; Vigneswaran, S. Mining Valuable Minerals from Seawater: A Critical Review. *Environ. Sci. Water Res. Technol.* **2017**, *3*, 37–53. [CrossRef]

38. Circular Processing of Seawater Brines from Saltworks for Recovery of Valuable Raw Materials. Available online: https://cordis.europa.eu/project/id/869467 (accessed on 1 January 2021).

39. Culcasi, A.; Gurreri, L.; Cipollina, A.; Tamburini, A.; Micale, G. A Comprehensive Multi-Scale Model for Bipolar Membrane Electrodialysis (BMED). *Chem. Eng. J.* **2022**, *437*, 135317. [CrossRef]

40. Romano, S.; Battaglia, G.; Bonafede, S.; Marchisio, D.; Ciofalo, M.; Tamburini, A.; Cipollina, A.; Micale, G. Experimental Assessment of the Mixing Quality in a Circular Cross-Sectional t-Shaped Mixer for the Precipitation of Sparingly Soluble Compounds. *Chem. Eng. Trans.* **2021**, *86*, 1165–1170. [CrossRef]

41. Schikarski, T.; Trzenschiok, H.; Peukert, W.; Avila, M. Inflow Boundary Conditions Determine T-Mixer Efficiency. *React. Chem. Eng.* **2019**, *4*, 559–568. [CrossRef]

42. Battaglia, G.; Romano, S.; Raponi, A.; Marchisio, D.; Ciofalo, M.; Tamburini, A.; Cipollina, A.; Micale, G. Analysis of Particles Size Distributions in Mg(OH)$_2$ Precipitation from Highly Concentrated MgCl$_2$ Solutions. *Powder Technol.* **2022**, *398*, 117106. [CrossRef]

43. Vicari, F.; Randazzo, S.; López, J.; Fernández de Labastida, M.; Vallès, V.; Micale, G.; Tamburini, A.; D'Alì Staiti, G.; Cortina, J.L.; Cipollina, A. Mining Minerals and Critical Raw Materials from Bittern: Understanding Metal Ions Fate in Saltwork Ponds. *Sci. Total Environ.* **2022**, *847*, 157544. [CrossRef]

44. Hanna, A.A.; Abdelmoaty, A.S.; Sherief, M.A. Synthesis, Characterization, and Thermal Behavior of Nanoparticles of Mg(OH)$_2$ to Be Used as Flame Retardants. *J. Chem.* **2019**, *2019*, 1805280. [CrossRef]

45. Meshkani, F.; Rezaei, M. Effect of Process Parameters on the Synthesis of Nanocrystalline Magnesium Oxide with High Surface Area and Plate-like Shape by Surfactant Assisted Precipitation Method. *Powder Technol.* **2010**, *199*, 144–148. [CrossRef]

46. Ardizzone, S.; Bianchi, C.L.; Fadoni, M.; Vercelli, B. Magnesium Salts and Oxide: An XPS Overview. *Appl. Surf. Sci.* **1997**, *119*, 253–259. [CrossRef]

47. Wang, J.A.; Novaro, O.; Bokhimi, X.; López, T.; Gómez, R.; Navarrete, J.; Llanos, M.E.; López-Salinas, E. Characterizations of the Thermal Decomposition of Brucite Prepared by Sol-Gel Technique for Synthesis of Nanocrystalline MgO. *Mater. Lett.* **1998**, *35*, 317–323. [CrossRef]

48. Verri, G. Process for the Purification of Magnesium Hydroxide. U.S. Patent 5,626,825, 6 May 1997.

49. Wu, X.F.; Hu, G.S.; Wang, B.B.; Yang, Y.F. Synthesis and Characterization of Superfine Magnesium Hydroxide with Monodispersity. *J. Cryst. Growth* **2008**, *310*, 457–461. [CrossRef]

50. Sierra-Fernandez, A.; Gomez-Villalba, L.S.; Milosevic, O.; Fort, R.; Rabanal, M.E. Synthesis and Morpho-Structural Characterization of Nanostructured Magnesium Hydroxide Obtained by a Hydrothermal Method. *Ceram. Int.* **2014**, *40*, 12285–12292. [CrossRef]

51. Henrist, C.; Mathieu, J.P.; Vogels, C.; Rulmont, A.; Cloots, R. Morphological Study of Magnesium Hydroxide Nanoparticles Precipitated in Dilute Aqueous Solution. *J. Cryst. Growth* **2003**, *249*, 321–330. [CrossRef]